

GT2011-45* &

NUMERICAL DESIGN AND EXPERIMENTAL EVALUATION OF AN AGGRESSIVE S-SHAPED COMPRESSOR TRANSITION DUCT WITH BLEED

A D Walker, A G Barker and J F Carrotte
 Dept. of Aeronautical and Automotive Engineering,
 Loughborough University, UK
 Email: a.d.walker@lboro.ac.uk

ABSTRACT

The ability to design S-shaped ducts with high aerodynamic loading is advantageous from a performance and/or weight saving perspective. However, the radial pressure gradients required to turn the flow produce strong pressure gradients in the axial direction. This promotes the likelihood of flow separation from the inner casing as the loading is increased. The current paper presents a novel approach to accommodating the increased loading by bleeding an amount of air from the critical inner casing. The process through which the air is bled re-energizes the boundary layer sufficiently to enable it to remain attached despite the high duct loading.

A bled duct is numerically developed and experimentally evaluated using a fully annular isothermal facility, with representative inlet conditions provided by a single stage axial compressor. The measurements indicate successful operation of this new design concept with a reduction in the overall system length, compared to a conventional design, of approximately 30% and a reduction in loss of approximately 20%. The data also demonstrate, to a limited degree, the ability to control the flow distribution at duct exit ultimately improving flow uniformity. Furthermore, the pressure of the bled flow is higher than at rotor exit where, in current engine architectures, flow is typically removed from the main gas path. In other words current engine bleed locations could be replaced by a bleed flow within the transition duct, and this flow is of sufficient pressure to meet the existing requirements associated with cooling, sealing and/or zone ventilation.

NOMENCLATURE

A	-	Area
B	-	Bleed
Cp	-	Static pressure rise coefficient
h	-	Passage height
H	-	Shape Factor (δ^*/θ)
IGV	-	Compressor Inlet Guide Vane
L	-	Duct length
m	-	Mass flow
N	-	Rotor speed
OGV	-	Compressor Outlet Guide Vane
P	-	Total pressure
p	-	Static pressure
r, R	-	Radius

r_m	-	Mean radius
r_i	-	Inner wall (hub) radius
r_o	-	Outer wall (casing) radius
T_u	-	Turbulence intensity (u'/\bar{U})
U, V, W	-	Axial, radial and tangential velocity components in cylindrical-polar coordinates
U_L, V_L	-	Velocity components relative to local traverse plane
x	-	Axial coordinate
α	-	Kinetic energy flux coefficient
δ	-	Flow deviation
δ^*	-	Boundary layer displacement thickness
ΔR	-	Change in radius
ρ	-	Density
ν	-	Modified viscosity
ϕ	-	Flow coefficient
ψ	-	Work coefficient
θ	-	Boundary layer momentum thickness
λ	-	Total pressure loss coefficient
τ_w	-	Wall shear stress
Superscripts:		
-	-	Area weighted spatial average
~	-	Mass weighted spatial average
ST	-	Streamtube
Subscripts:		
1-5	-	Measurement planes
L	-	Local plane

INTRODUCTION

To optimize the performance of multi-spool gas turbine compressor systems the diameter of each spool must reduce as the air density increases. In order to accomplish this, the annular transition duct connecting the low and high pressure compressor spools generally takes the form of an S-shape. In modern, high pressure ratio aircraft engines this radius change is increasing and must be accomplished in the shortest possible length to minimize engine length/weight. Consequently there is a need to design progressively more aggressive S-shaped ducts. However, within such ducts flow separation must be avoided if, in line with overall cycle performance, the stagnation pressure loss is to be minimized and the downstream compressor performance not adversely affected. Furthermore, what appears to be a relatively simple geometric shape actually poses some

significant aerodynamic challenges. This is because of the complex nature of the flow fields that develop under the combined influence of pressure gradient and streamline curvature effects.

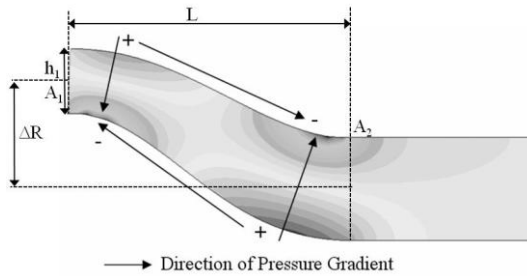


Figure 1: Static Pressure in an S-Shaped Duct

As the flow follows a curved path through the duct a modification to the static pressure field occurs (Figure 1). Across the first bend a radial pressure gradient is required to turn the flow inwards such that the pressure close to the outer casing is higher than that adjacent to the inner. Within the second bend the flow is returned to the axial direction and so this radial pressure gradient is reversed. As a consequence streamwise pressure gradients are generated that influence the flow field development in various regions of the duct, including the boundary layers that develop along the duct walls. In particular, for a compressor transition duct this means that the flow is subject to an adverse pressure gradient along most of the inner casing, with an increasing likelihood of separation within the 2nd bend. Several basic parameters can be used to quantify, geometrically, the aggressiveness of an S-shape duct. For example, with reference to Figure 1, the non-dimensional radius change ($\Delta R/L$) reflects the severity of the curvature induced pressure gradients. The duct area ratio (A_2/A_1) reflects the bulk deceleration (or acceleration) of the fluid and, in a similar way to a conventional diffuser, the non-dimensional length (L/h_1) over which this is undertaken will dictate the axial pressure gradient. These combine to set the magnitude of the adverse pressure gradient along the inner wall of the second bend where separation is most likely. For the current work duct length alone was reduced to increase overall loading. However, as highlighted in the following discussion other aerodynamic factors should also be considered such as the duct inlet conditions (turbulence structure, boundary layer thickness etc.) and exit conditions.

In addition to pressure gradient effects the turbulent flow field is directly influenced by the streamline curvature that is undertaken by the flow. As described by Bradshaw^[1] the imbalance that exists between the centripetal acceleration of a turbulent fluid element and the surrounding pressure field gives rise, over a convex surface, to reduced turbulence levels so that turbulent mixing is inhibited and turbulent stresses reduced. Alternatively, over a concave surface turbulent mixing and the associated stresses are increased. Hence modification to the turbulent flow field by streamline curvature effects can be of significance, particularly in regions where the flow is close to separation. For example, along the inner wall turbulence

suppression in the first bend reduces the exchange of momentum close to the casing surface making the flow more prone to separate. However, the turbulent enhancement in the second bend increases this beneficial momentum exchange reducing the likelihood of separation, although it takes some distance (order 2 boundary layer heights^[2]) for the effects to be observed in the mean velocity field.

Numerous studies have investigated the complex flow development within S-shaped ducts. For example, in a series of work Britchford et al.^[2, 3, 4] and Bailey et al.^[5, 6, 7] assessed the performance of a modestly loaded annular S-shaped duct, quantifying its mean flow and turbulence structure in addition to investigating the effect of compressor generated inlet conditions. The presence of an upstream compressor, and in particular the presence of outlet guide vane (OGV) wakes, can have a notable effect on the duct performance. Britchford et al.^[2] and Karakasis et al.^[8] both measured a notable increase in loss between “clean” and compressor generated inlet conditions. However, the increased turbulent mixing can also be beneficial as it promotes the transfer of higher momentum core flow into the boundary layer. This phenomenon has been utilized for many years to enable the design of more aggressive combustor pre-diffusers (see for example Carrotte et al.^[9]). In S-shaped ducts the increased turbulent mixing has also been observed to offset duct loading but the phenomenon is modified by the radial pressure gradient present in the first bend. Karakasis et al.^[8] reported that the wake mixing causes the hub boundary layer fluid to be pumped into the higher velocity free stream thereby replacing it with more energetic fluid. In an earlier investigation Britchford^[2] also reported this commenting that the radial pressure gradient affects the low momentum wake fluid to a greater extent than the core flow, thereby driving it towards the inner casing. Although the wake flow has lower total pressure than the core flow it is still higher than the boundary layer and thus acts to re-energize the latter. Ultimately the presence of compressor generated inlet conditions enables a more aggressive S-shaped duct to be used.

Recently, to facilitate more aggressive duct designs the European Union commissioned the AIDA project^[10] with the goal of 20% shorter ducts or a 20% increase in radius change. Within this project Ortiz Duenas et al.^[11] studied the effect of reducing length on the performance of a planar S-shaped duct highlighting a rapid increase in loss as the duct becomes shorter and the flow approaches separation. This study highlights the limit in aerodynamic loading that can be achieved in conventional S-shaped ducts. Consequently, other authors have applied a range of techniques to design more aggressive ducts which do not separate. Walker et al.^[12] utilized an integrated design concept to incorporate the upstream outlet guide vane row into the first bend of an S-duct thereby saving 20% in length. Wallin and Errikson^[13], Naylor et al.^[14] and Karakasis et al.^[8] all designed notably more aggressive ducts through the use of end-wall contouring, shape optimization and non-axisymmetric designs. Santner et al.^[15] reduced the separation in a 2D S-duct by employing low-profile vortex generators to energize the boundary layer. However, they found that the same

vortex generators had little effect when blade wakes and secondary flows were present in the inlet flow.

In the current investigation a novel bleed was employed to re-energize the boundary layer immediately upstream of the critical second bend on the inner wall of an S-shaped duct. The concept was derived from the work of Walker et al.^[16, 17] who employed the technique to achieve very high rates of diffusion in combustor pre-diffusers. This so called Hybrid diffuser (Figure 2) utilizes bleed flow in a specific manner that enables the wall boundary layer to remain attached under aerodynamic loading that would normally result in separation. Walker et al.^[16] revealed that the controlling flow mechanism is not a simple boundary layer bleed but involves a more complex interaction between the accelerating bleed flow and the diffusing mainstream flow.

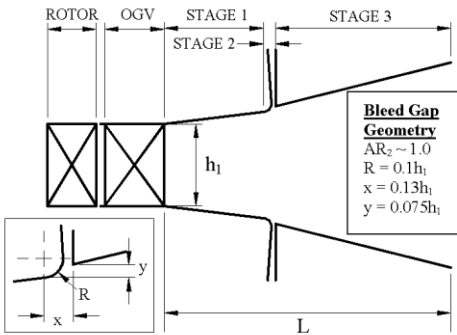


Figure 2: Hybrid Diffuser, Walker^[16]

The two governing processes are indicated in Figure 3. Firstly, the bleed flow gains streamwise momentum as it accelerates into the bleed duct. A turbulent shear layer exists between the accelerating bleed flow and the diffusing mainstream flow. Streamwise momentum is transported, across this layer, to the diffusing mainstream flow, re-energizing it and enabling it to remain attached on the high angle downstream wall. Secondly, the radial pressure gradient created by the bleed causes deflection of the mainstream flow and enhances further the transport of higher momentum fluid into the boundary layer. In combustor pre-diffusers Walker et al.^[16] noted that, for a given aerodynamic loading (i.e. area ratio) there was a minimum bleed requirement above which little extra benefit was gained. However, it was noted that higher levels of bleed could be used to manipulate the radial profile “pulling” the bulk flow towards the bleed which could be useful in removing unwanted bias. In modern gas turbine engines use of a bled system depends very much on the ability to utilize the bleed air in a meaningful way. For example, Walker et al.^[16] suggested the bleed from their hybrid diffuser could be used in component cooling. Upstream of a compressor S-shaped duct there is typically an inboard bleed flow which, potentially, could be replaced by one located within the transition duct.

Employing this type of bleed in an S-shaped duct presents some additional challenges. It is not obvious where the bleed should be located; along the inner wall the flow is subject to varying pressure gradients both in a streamwise and radial

sense which may well alter the mechanisms described above. Further, the wall angle itself is much higher than seen in a combustor diffuser. Ultimately this necessitated the use of a preliminary CFD study to find the best location for the bleed.

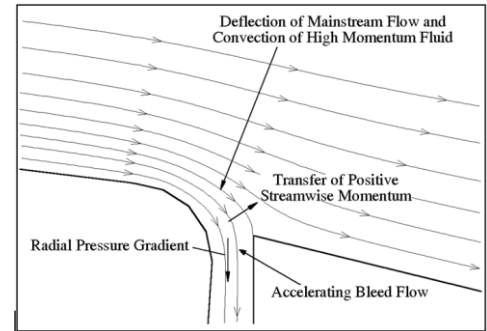


Figure 3: Mechanisms of a Hybrid Diffuser, Walker^[16]

BASELINE DUCT DESIGN

A sensible datum design would be an aggressive but conventional S-shaped duct. However, Walker et al.^[12] already demonstrated a 20% length reduction for such a design by integrating the OGV row into the first bend of an otherwise conventional design. The geometric parameters of both these ducts are shown in Figure 4 (conventional datum and IOGV). Thus, in the current study, the IOGV design was used as the baseline from which to develop a bled duct (although the conventional datum was used for some preliminary work). Consequently, the system can now be thought of as a fully integrated concept; integrating firstly the OGV row into the duct but also, if successful, integrating the local engine bleed requirements into the transition duct.

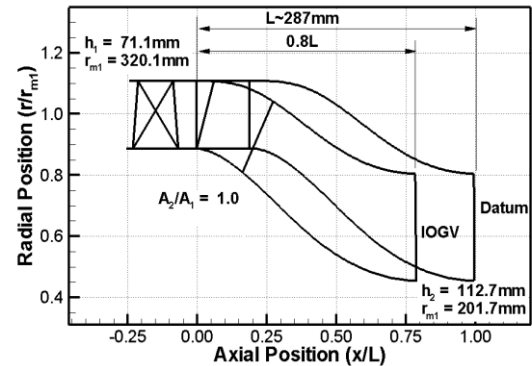


Figure 4: Conventional Datum and Integrated OGV S-Ducts, Walker et al.^[12]

NUMERICAL METHODOLOGY

In line with the complex aerodynamics within an S-shaped duct the accurate numerical prediction of the flow field provides a notable challenge. The choice of modeling strategy is crucial. For example turbulence models such as Spalart-Allmaras and k- ω SST have been shown (by by Ortiz-Dueñas et al.^[11] and Karakasis et al.^[8]) to give solutions which differ from experimental data in the near wall regions. This is not surprising as eddy-viscosity models use the Boussinesq

hypothesis to compute the Reynolds stresses. This assumes isotropic turbulent viscosity which is certainly not the case in the presence of strong streamline curvature. Britchford et al.^[4] showed that a Reynolds stress transport model is able to capture some impact of streamline curvature on the turbulence field, although the predicted data still showed some minor differences to measured data. Furthermore, with compressor generated inlet conditions wake mixing through the transition duct must also be correctly captured in order to obtain the correct wake characteristics and therefore any radial migration of wake fluid towards the critical inner wall. Eddy-viscosity models have been observed to be less accurate in unconfined flows such as far wakes and mixing layers as the rate of turbulent kinetic energy production can be much less than the rate of dissipation. In studying the integrated OGV concept Walker et al.^[12] achieved relatively good agreement between predicted and measured data using the commercial CFD code Fluent (v6.3), a Reynolds stress turbulence closure and standard wall functions. Hence a similar numerical methodology was employed here to model the S-shaped duct flow downstream of the OGV row. A simple 2D duct model was used to assess loading and develop preliminary bled duct designs which were then assessed on a 3D model (Figure 5). Since the baseline duct sits downstream of a compressor containing 48 OGV the computational domain for the 3D model was reduced to a 7.5° sector with periodic end walls. Downstream of the duct it wasn't feasible to include realistic engine geometry (i.e. a compressor) but it was noted that the downstream geometry has the potential to modify the duct flow. Therefore a settling length equal to 3.5 duct exit heights was used both in the CFD and experiment. This was sufficient to ensure the static pressure profile emanating from the ducts became radially uniform.

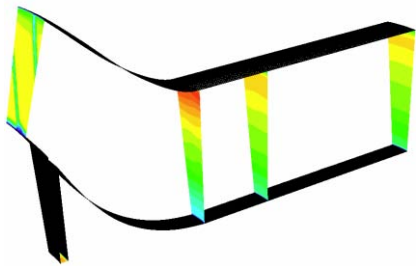


Figure 5: Example 7.5° Sector CFD Model

Velocity inlet conditions were taken from the five-hole probe measurements made by Walker et al.^[12] at OGV exit in both the Datum and IOGV ducts. An example of the IOGV 3D inlet condition is shown (Figure 6). Similarly, turbulence data were computed from the corresponding hot-wire data. It must be noted that this methodology omits the unsteadiness generated by the rotor wakes which will be present in both an engine and the test facility. However, it is likely that the effect of this would be most notable in the OGV row rather than in the downstream duct. Additionally, with the inlet conditions generated from the measured OGV exit data, modification of the mean flow field should be included; at least sufficiently for a time-averaged prediction. It should be noted that in deriving

the turbulence intensity and length scale from the measurements the rotor passing frequency was removed using the method of Camp and Shin^[18]. In this way the mean turbulence was a true reflection of the mean flow field and not artificially increased by the rotor passing frequency and its harmonics.

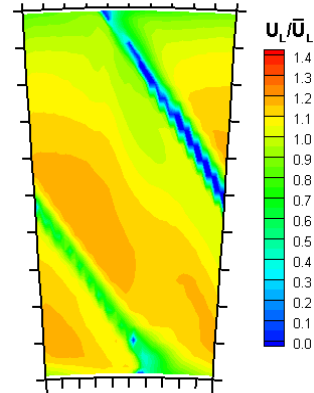


Figure 6: 3D CFD Inlet Conditions – IOGV

PRELIMINARY DESIGN CALCULATIONS

In order to demonstrate the bled duct concept a number of preliminary numerical predictions were undertaken aimed at defining the bleed geometry, its location and the actual amount of bleed required. To do this a 2D axi-symmetric model based on the datum duct was used. Without the complexity of integrated OGV it was easier to parametrically alter the duct loading (i.e. reduce the length) via the simple trigonometric equation used to define its geometry^[2]. Although the omission of the OGV will affect the performance of the downstream duct it is unlikely this will affect the final geometry and position of the bleed. The minimum bleed requirement to prevent separation will depend on the aggressiveness of the duct. Alternatively, one could ask how aggressive or how much shorter can a duct be made for a specific level of bleed? Typical bleed flows in the vicinity of a compressor transition duct are around 3-5% of the mass flow so this seemed a logical starting point. The axi-symmetric predictions showed that simply reducing the length (L) whilst maintaining the radius change (ΔR) resulted in a rapid increase in loss and exit profile distortion, followed by separation when the length was reduced to less than 0.9L (Figure 7).

Consequently, a preliminary bled duct was specified, based on the conventional datum, with the length reduced to 0.8L. The geometry of the bleed off-take was designed in line with the parameters specified by Walker^[16, 17] (see Figure 2) and it was found, after several iterations, that the best location for the bleed was at approximately 35-40% of duct length. This locates the bleed immediately upstream of where an un-bled duct would separate and at the point where the static pressure gradient has become strongly adverse. Velocity contours (see Figure 7) suggest that at this reduced length the duct remains fully attached with a bleed rate of 3%.

Unfortunately as S-shaped ducts become more aggressive the deviation (see Figures 8) between the actual and geometric

turning increases. In other words there is residual turning downstream of the duct, a redistribution of the flow and a static pressure profile that the downstream compressor must accommodate. Figure 9 illustrates the effect of bleed on the predicted deviation within two ducts of length $0.8L$ and $0.9L$. (As before L is the length of the conventional datum). It shows that for a given bleed the deviation from the geometrical turning increases with reduced length but also that this deviation is reduced with increased bleed. Similarly, Figure 10 shows the effect of this on the duct exit velocity profile. At 0% and 1% bleed the shape factor would suggest the inner wall boundary layer is close to separation. However, with increased bleed the condition of the inner wall boundary layer and the overall uniformity of the profile significantly improved.

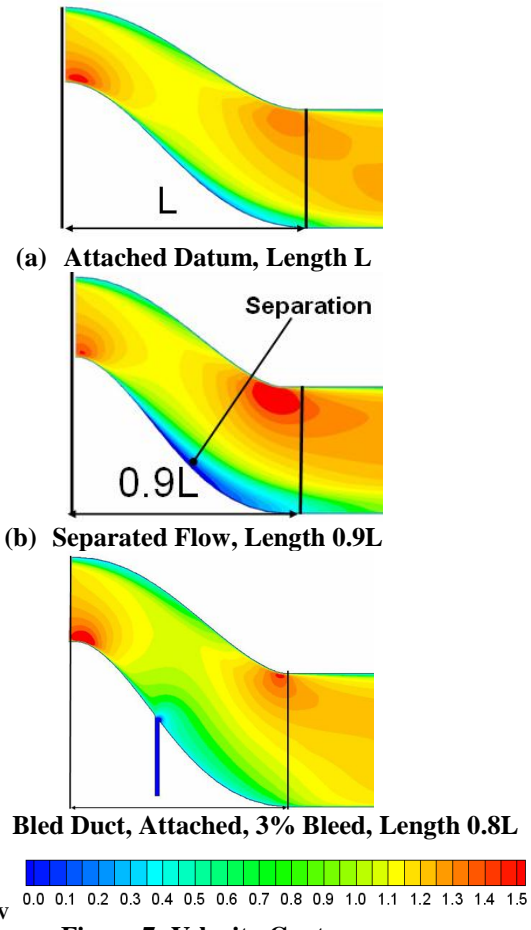


Figure 7: Velocity Contours

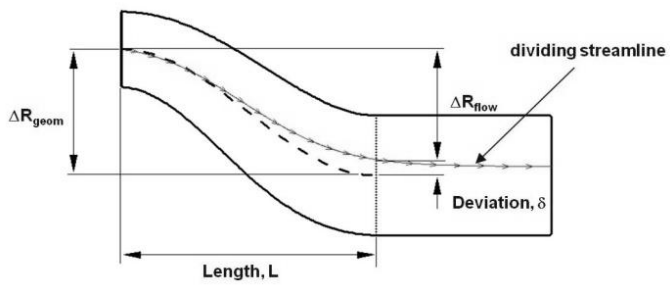


Figure 8: Flow Deviation

Ideally an IOGV row would be designed mutually with the downstream bled duct. However, to reduce costs the original IOGV row of Walker et al.^[12] was retained and two candidate bled ducts specified to fit downstream of this. With reference to the conventional datum duct these two designs reduced the overall system length (from OGV inlet) by close to 30% and 40% respectively (see Figure 11). 3D predictions were undertaken to assess both and Figure 12 compares the inner wall axial shear stress to the datum and un-bled IOGV designs (both of which have been shown experimentally^[12] to be close to be not actually separated). In the critical second bend the shorter of the two candidates (#2) had a predicted inner wall shear stress lower than that of the datum and as such was deemed to be too aggressive. Thus only candidate #1 was taken forward to manufacture and experimental assessment.

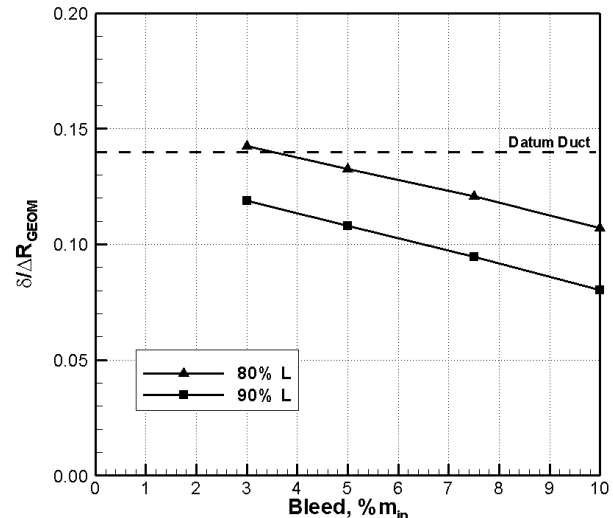


Figure 9: Effect of Bleed on Deviation

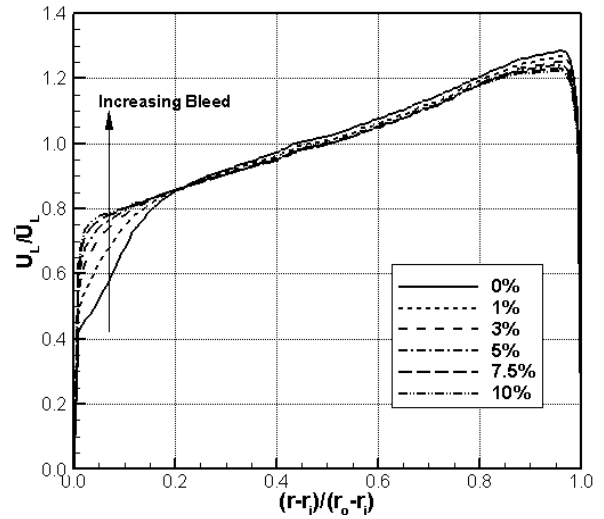


Figure 10: Predicted Effect of Bleed Rate on Exit Profile

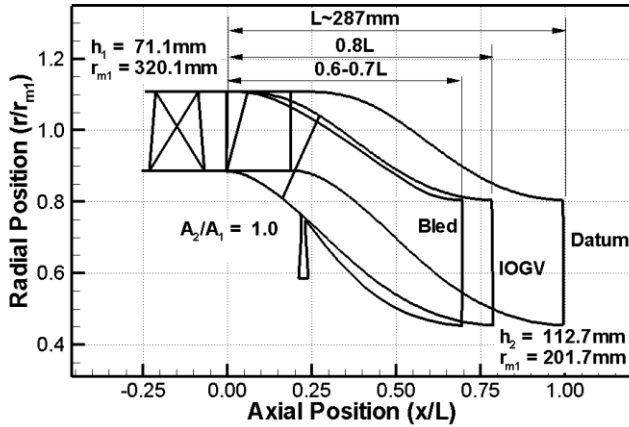


Figure 11: Bled, IOGV and Datum Ducts

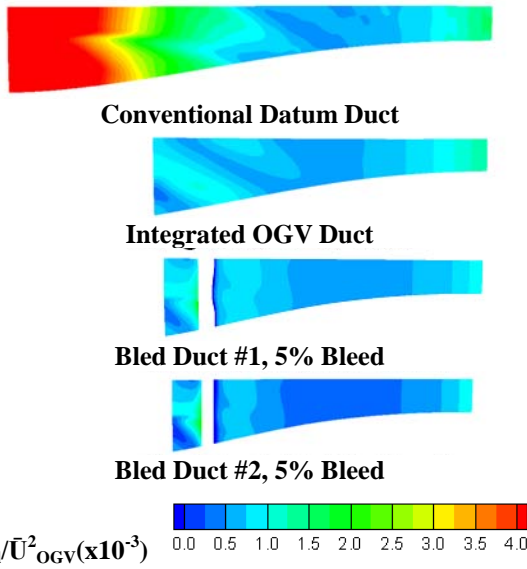
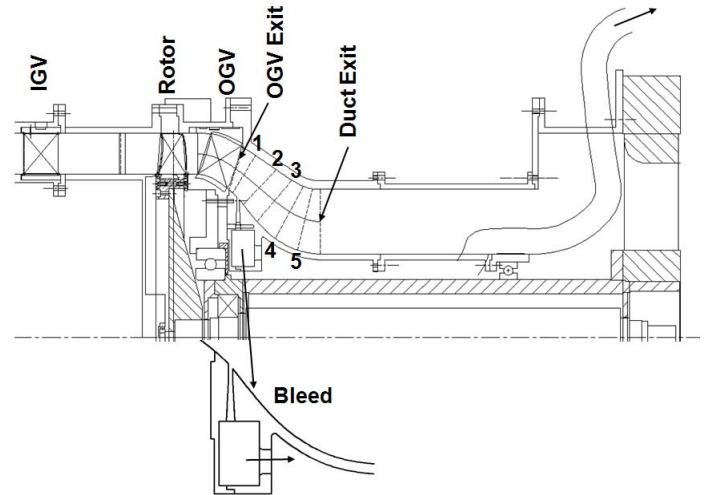


Figure 12: Predicted Wall Shear Stress

EXPERIMENTAL FACILITY

All experimental data were obtained on a low speed isothermal test facility operating at nominally atmospheric conditions (Figures 13-14). Air was drawn into a large inlet plenum above the vertically mounted facility, before passing through an inlet flare and honeycomb flow straightener. The air was then accelerated over a bell-mouth intake section prior to entering the test section which consisted of an IOGV row and compressor rotor along with the transition duct (within which the IOGV row has been integrated). The mean radius of the IOGV and rotor was 320.1mm with a passage height of 71.1mm (h_1). The IOGV row provided 10° of swirl onto the rotor which operated at a fixed non-dimensional mass flow condition ($m\sqrt{(RT)}/AP$) and speed ($(N\pi D)/\sqrt{(\gamma RT)}$). This corresponded to a flow co-efficient (Va/U) of $\phi = 0.55$ and a work coefficient ($\Delta H/U^2$) of $\psi = 0.4$ giving a mass flow of $6.3\text{kg}\cdot\text{s}^{-1}$. The blade loadings were designed to be typical current engine practice and, for in test rig, resulted in an axial velocity through the blade rows of approximately 33ms^{-1} (Mach No. 0.1).

Cumpsty^[19] reports that for IOGV Reynolds numbers below 1.5×10^5 an undesirable separation bubble may develop on the suction surface of the IOGV. In the present experiment the IOGV Reynolds number was in excess of 2.0×10^5 and therefore sufficiently high to avoid this. Further, the Reynolds number sensitivity of the IOGV row was also suppressed by the presence of the relatively high levels of turbulence ($>3\%$) generated by the rotor. Consequently, the wake mixing within the downstream S-shaped duct was well represented. As mentioned previously the IOGV row was retained from the study of Walker et al.^[12]. However, downstream of the IOGV row the modified bled duct geometry incorporated an annular bleed slot (supported by several internal struts) and associated bleed chamber (see Figure 13). A separate fan with a calibrated inlet section was used to supply the necessary change in pressure required to control the amount of flow being removed from the transition duct. This enabled a variety of bleed flow rates to be investigated. Downstream of the S-shaped duct it was beyond the scope of the current work to include an engine representative compressor. Thus, as in the CFD a settling length equal to 3.5 duct exit heights was used. This was sufficient to ensure the static pressure profile emanating from the ducts became radially uniform before the flow passed into a sub floor plenum and then through a centrifugal fan before exhausting to atmosphere. The combination of the throttle and fan were used to maintain the desired compressor operating condition.



	1	2	3	4	5	Exit
x/L	0.31	0.38	0.51	0.75	0.88	1.0

Figure 13: Bled S-Duct Test Section and Traverse Planes

Information on the mean flow field was obtained using miniature five-hole pressure probes, of approximately 1.75mm diameter, calibrated and employed in a non-nullled mode as outlined by Wray and Carrotte^[20]. Measurements were performed on the planes shown in Figure 13. (The axial location, x/L, is with respect to the duct inlet). Each plane was aligned normal to the duct centre line and movement of the probe, across the annular passage, was obtained using a linear

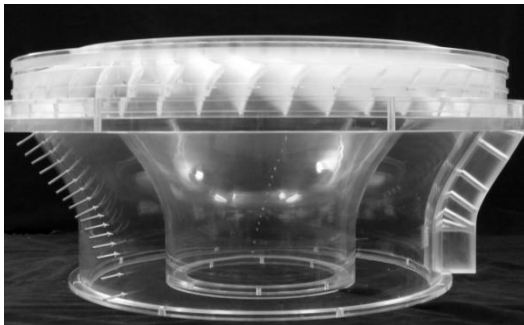
stepper motor. Circumferential movement was obtained by mounting the IGV and OGV rows within carrier rings such that the blade rows could be indexed circumferentially.



(a) Rig Assembly (Datum)



(b) IOGV



(c) IOGV and Duct

Figure 14: Test Rig Photographs

DATA REDUCTION AND ERRORS

All the measurements were corrected to standard day conditions ($P_{amb} = 101325 \text{ Nm}^{-2}$, $T_{amb} = 288.15 \text{ K}$) and in all cases the velocities were measured in a local co-ordinate system (Figure 15). This consisted of vectors normal to the

traverse plane (U_L), in the line of the measurement plane (V_L) and circumferentially around the duct (W_L). Typically data is presented in this local format since it enables the development of the flow within the duct to be more easily understood. The 5-hole probe area traverses provided local total and static pressures in addition to the velocity vector. Therefore, at a given plane, spatially averaged values can be obtained through suitable averaging techniques. The spatially averaged velocity normal to the traverse plane (\bar{U}) was obtained by area weighting the individual values while the total (\bar{P}) was mass weighted such that:

$$\bar{P} = \bar{p} + \alpha \frac{1}{2} \rho \bar{U}^2 \quad \text{and} \quad \alpha = \frac{1}{A} \int^A \left(\frac{u}{\bar{U}} \right)^3 \quad (1)$$

Where α is the kinetic energy coefficient and compares the kinetic energy flux of the actual profile to a uniform profile with the same mass flow. Hence, changes in the spatially averaged pressures between any two planes can then be expressed in terms of a total pressure loss (λ) and static pressure rise coefficient (C_p), with the change in pressures being non-dimensionalised by a suitable reference dynamic pressure.

$$\lambda = \frac{\bar{P}_1 - \bar{P}_2}{\bar{P}_1 - \bar{p}_1} \quad \text{and} \quad C_p = \frac{\bar{p}_2 - \bar{p}_1}{\bar{P}_1 - \bar{p}_1} \quad (2)$$

In this way, for example, the mass-weighted duct loss can be obtained using the duct inlet (plane '1') and duct exit (plane '2') traverse plane data. However, for the bled ducts the impact of the removal of flow from the transition duct should also be considered. This flow is typically of low pressure and so, using the aforementioned analysis, a low duct pressure loss could be potentially indicated which merely reflects the removal of relatively low pressure air via the bleed slot. An alternative method is therefore to apply the above analysis on a streamtube basis (Figure 16). Although this assumes there is no radial redistribution of fluid it is thought that this method goes some way to accounting for the flow that is removed. Based on the percentage flow that enters the bleed slot a streamtube can be defined and a mass weighted total and static pressure calculated for this streamtube from which a loss can be defined:

$$\lambda = \frac{\bar{P}_{1_ST} - \bar{P}_{2_ST}}{\bar{P}_{1_ST} - \bar{p}_{1_ST}} \quad \text{and} \quad C_p = \frac{\bar{p}_2 - \bar{p}_{1_s}}{\bar{P}_1 - \bar{p}_{1_s}} \quad (3)$$

The general accuracy of the rig hub and casing dimensions was measured, typically, to be of order 0.1mm and at each traverse plane the traverse height was also measured and found to be within 0.2% of that specified. The positional accuracy of the 5-hole pressure probe was within 0.1mm radially and 0.1° circumferentially and the pressures measured were estimated to be accurate to within 1%. The total velocity of the flow was obtained from the dynamic pressure, and hence the accuracy of the local velocities was within $\pm 0.5\%$. Whilst the pitch angle of the flow was determined from the calibration of the probe, additional errors in yaw angle could arise associated with the ability of the user to align the probe with the rig centre line. It is estimated that this could be set to within 1°, and this level of

accuracy was reflected in the measured swirl angles and circumferential component of velocity. In addition to the errors associated with the local measurements it was estimated that the mass weighted total and static pressures at a given traverse plane were repeatable to better than 10Pa. The calculated mass flows at each traverse plane, derived from the velocity measurements, were all within 2.5% of each other.

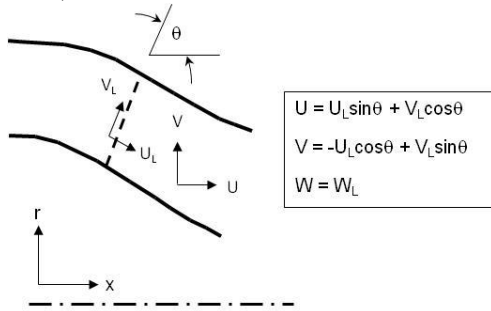


Figure 15: Local Co-ordinate System

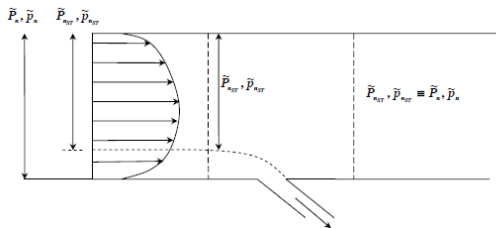


Figure 16: Streamtube Based Loss Analysis

RESULTS AND DISCUSSION

(i) Overall Flow Field Development

Results are initially presented for the design bleed where 5% of the flow entering the S-shaped duct is bled through the slot on the inner casing. The development of the circumferentially averaged velocity profile (normal to the traverse plane) is illustrated in Figure 17. Not surprisingly a similar flow field is observed upstream of the rotor (not presented) for both the bled and un-bled configurations resulting in the rotor being presented with the same flow conditions. In addition the flow fields measured at OGV inlet are also similar. However at OGV exit some slight differences are apparent in the measured data which may be due to the upstream influence of the bleed slot along with differences in the downstream duct curvature. Downstream of the OGV it becomes more difficult to directly compare the un-bled and bled designs due to differences in the traverse plane locations and the duct curvature. For both ducts the OGV exit profile is relatively flat but as the flow develops through the ducts a casing bias is generated by curvature induced pressure gradients. This is an inviscid affect and dominates the development of the profile in the so-called inviscid core region (i.e. away from the viscous dominated boundary layer flows). On the outer wall the boundary layer develops under the influence of a favorable pressure gradient and although the convex curvature in the second bend will act to enhance growth it remains relatively thin (<10-15% of passage height). On the

inner wall the pressure gradient is adverse and the boundary layer grows rapidly. However, the data clearly show the benefit of bleed and a reduced boundary layer growth relative to the un-bled IOGV duct. For example at plane 1, just upstream of the bleed, the profile close to the inner casing reflects the acceleration undertaken as the flow enters the bleed slot, accounting for the localized increase in the normal velocity. The boundary layer thickness for the bled duct is perhaps 10% of the passage height whereas for the un-bled duct it is closer to 20%.

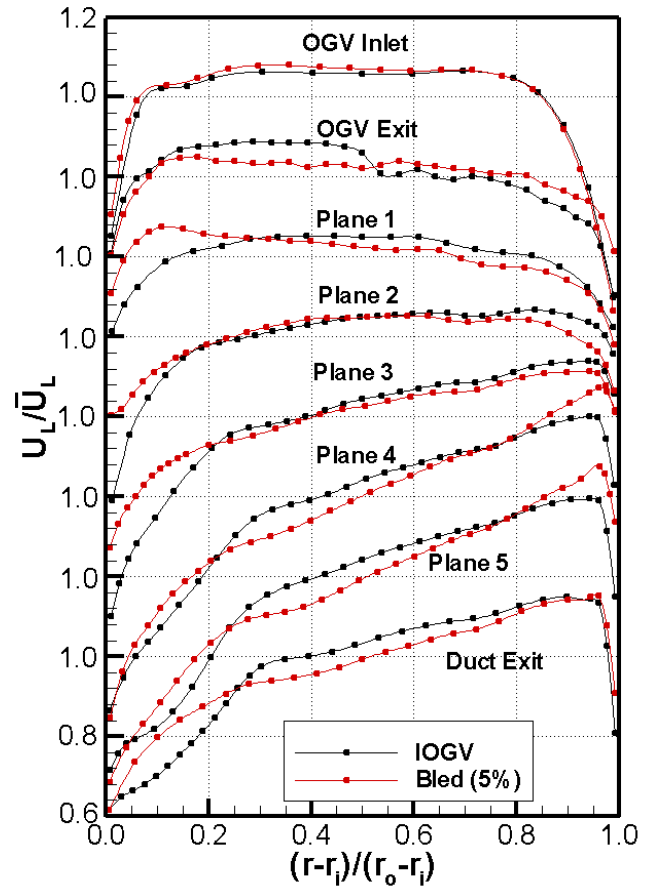


Figure 17: Circ. Averaged Profiles of Normal Velocity

Downstream of plane 1 and along the remaining length of the inner wall there is continued evidence of higher momentum flow. This is due partly to the removal of low quality flow through the bleed but mainly to the momentum transfer that occurs from the accelerating bleed flow to the adjacent mainstream flow which then forms the new boundary layer. Plane 3 represents the location where the critical inner wall flow is closest to separation. It is difficult to use a shape factor^[20] as the flow is three dimensional and contains blade wakes. However, the circumferentially averaged profiles presented in Figure 17 certainly suggest that the inner wall shape factor, H, for the un-bled IOGV duct, at planes 3 to 5, increases above 2.0-2.3 indicating separation is close. Furthermore, it is highly likely the time-averaged nature of the measurements may mask some transient separation. However,

for the bled duct the shape factor would appear to remain below 2.0 and results in the inner wall flow being much less likely to separate for despite the reduced length. At duct exit the outer wall boundary layers are nominally the same thickness (~5-10% of passage height). On the inner wall the bled duct has a significantly thinner boundary layer than the un-bled duct (~15-20% of passage height compared to ~30%) Moreover the profiles suggest that the shape factor for the bled duct is certainly below 2.0 whereas for the un-bled IOGV duct it is approaching 2.3-2.4.

(ii) Effect of Bleed Flow Rates on Duct Exit Profile

The effect of bleed flow rate on the flow within the transition duct was also assessed for a variety of rates ranging from 0% to 5% (increments of 1%), and also at 7.5% (the highest bleed rate attainable). The effect on the duct exit profile and velocity contours is illustrated in Figures 18 and 19. With 0% bleed the profile suggests that the exit flow is worse than the longer un-bled IOGV duct (see Figure 17). Furthermore, the profile suggests a shape factor in excess of 2.0 and the possibility of some transient behavior. Indeed examination of the normal velocity contours measured at plane 3 (Figure 20) highlights the presence of a localized region of very low velocity and demonstrates that the inner wall flow is probably separated.

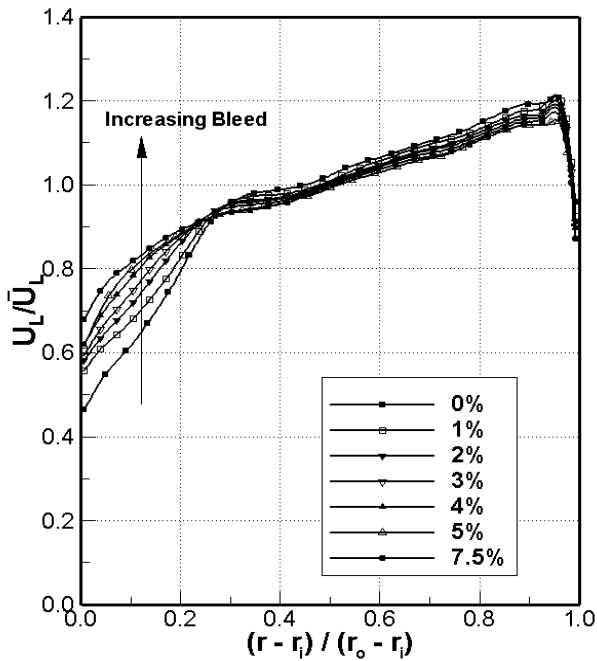


Figure 18: Effect of Bled Rate on Duct Exit (H) Profile

As the bleed rate increases it is clear that a strong influence is exerted over the inner 30% of the duct height. The profiles suggest the minimum bleed requirement is somewhere in the region of 2-3% but as the bleed increases further the inner wall boundary layer becomes notably smaller and the shape factor decreases. The contours at plane 3 also suggest that at 2% bleed the low velocity region close to the inner wall is almost eliminated. At the highest bleed rate the inner profile shows a

notable improvement over the lower bleed cases although the overall profile still exhibits significant bias generated by the duct curvature. The measured duct exit profiles (Figure 18) agree broadly with the preliminary predictions (Figure 10) but show a slightly larger inner wall boundary layer. This is probably due to the 2D axi-symmetric nature of the prediction which removes the secondary flows and their effects on the inner wall boundary layer. Example contours from the post-test 3D CFD prediction conducted using the measured inlet data to define the duct inlet condition are presented in Figures 19 and 21. These show a good level of agreement with the measured data both in terms of the near wall flows and general flow structures. A more comprehensive comparison is beyond the scope of the current paper.

(iii) System Performance

Across the OGV row the loss coefficient, λ , is approximately 0.05 which not surprisingly is, within experimental error, the same that was measured for the un-bled IOGV configuration (i.e. the same vane row). As previously mentioned, for the bled duct itself it is important to account for the flow, of relatively low total pressure, that is removed through the bleed slot when assessing duct performance. Hence based on a streamtube analysis the loss coefficient for the OGV (excluding 5% of the inboard flow associated with the bleed stream tube) is 0.045 and for the system this increases to 0.064 (from OGV inlet to duct exit). Overall the data suggest the system loss is less than that measured for the un-bled IOGV duct (0.083), although the absolute loss differences are relatively small.

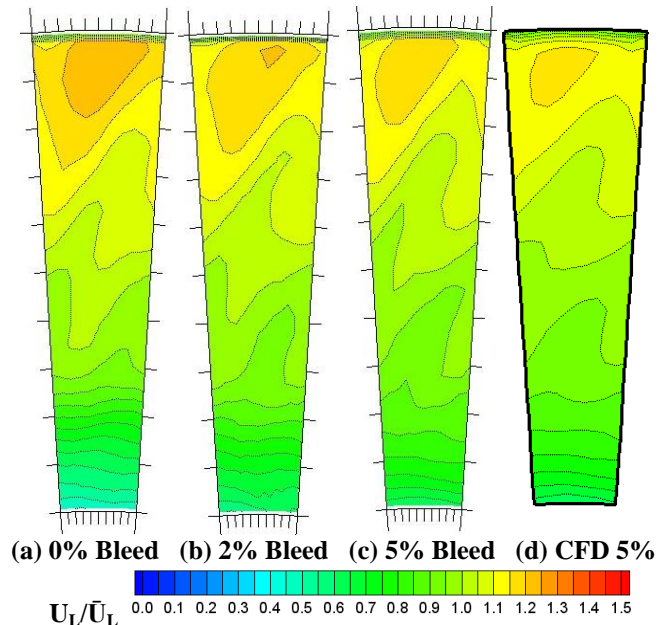


Figure 19: Effect of Bleed at Duct Exit

In addition to the transition duct loss, the loss between OGV inlet and the bleed cavity chamber was also measured. In current engine configurations flow is typically bled from the upstream exit of the rotor. Hence it is worth noting that the

bleed cavity pressure is higher than the rotor exit static pressure. This is due to the rise in static pressure through the OGV and in the transition duct (upstream of the bleed slot). Hence the bleed flow is of higher quality than if it had been removed at rotor exit (where the bleed pressure is more likely to approximate that of the static pressure at this location). Ultimately this suggests that the bleed flow from within the duct could replace and be used for the same purpose as the rotor exit bleed.

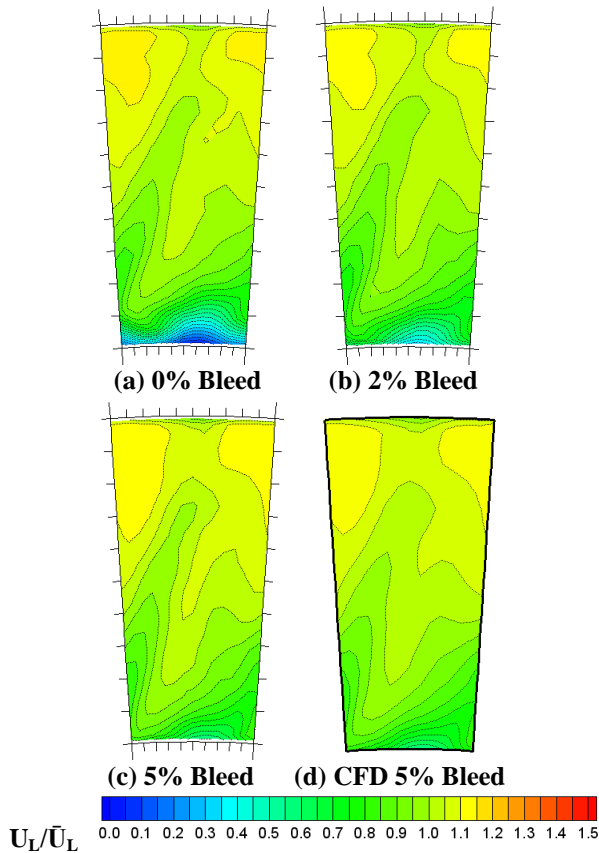


Figure 20: Effect of Bleed at Plane 3

CONCLUSIONS

A novel bleed has been employed to prevent flow separation in an aggressive S-shaped compressor transition duct. Numerical predictions were used to optimize the bleed location and its geometry for a 5% (design) bleed flow rate. Predicted data suggested the S-duct remained fully attached at an aerodynamic loading far above conventional levels giving a potential length reduction of 30-40% from conventional designs. Consequently, the performance of a bleed duct was experimentally evaluated on a fully annular isothermal test facility incorporating a single stage axial compressor. The experimental measurements confirmed that at the design bleed rate the flow was fully attached, and compared to a state-of-the-art integrated OGV design the system loss was reduced by approximately 20%. Without bleed the measurements suggested that the flow in the transition duct separated on the inner wall of the critical second bend. However, the data also suggested

that the flow reattached at a minimum bleed of 2-3%, i.e. less than the design bleed. Increasing the bleed rate further has a notable beneficial effect on the inner wall boundary layer and, to a limited degree, demonstrated the ability to control the flow distribution at duct exit. Furthermore, the pressure of the bleed flow was seen to be higher than that at rotor exit where, in current engine configurations, bleed flow is typically removed from the main gas path. This suggests that the bleed within the duct could replace the rotor bleed and be used, say, for zone ventilation.

ACKNOWLEDGMENTS

The authors wish to acknowledge the financial support of the European Commission. This work was conducted within the EU 6th Framework Project AIDA (Aggressive Intermediate Duct Aerodynamics for Competitive and Environmentally Friendly Jet Engines – Contract No. AST3-CT-2003-502836).

REFERENCES

- [1] Bradshaw, P., "The Effects of Streamline Curvature on Turbulent Flow", AGARD AG-169, 1973.
- [2] Britchford, K. M., 1998, "The Aerodynamic Behavior of an annular S-Shaped Duct", PhD Thesis, Loughborough University, UK.
- [3] Britchford, K. M., Carrotte, J. F., Stevens, S. J. and McGuirk, J. J., 1994, "The Development of the Mean Flow and Turbulence Structure in an Annular S-Shaped Duct", ASME 94-GT-457.
- [4] Britchford, K. M., Manners, A. P., McGuirk, J. J. and Stevens, S. J., 1994, "Measurement and Prediction of Flow in Annular S-Shaped Ducts", J. of Exp. Thermal and Fluid Science, 9(2), pp. 197-205.
- [5] Bailey, D. W. and Carrotte, J. F., 1996, "The Influence of Inlet Swirl on the Flow within an Annular S-Shaped Duct", ASME 96-GT-60.
- [6] Bailey, D. W., Britchford, K. M., Carrotte, J. F. and Stevens, S. J., 1997, "Performance Assessment of an Annular S-Shaped Duct", ASME J. of Turbomachinery, 119 (1), pp. 149-156.
- [7] Bailey, D. W., 1997, "The Aerodynamic Performance of an Annular S-shaped Duct", PhD Thesis, Loughborough University, UK.
- [8] Karakasis, M. K., Naylor, E. M. J., Miller, R. J., and Hodson, H. P., 2010, "The Effect of an Upstream Compressor on a Non-Axisymmetric S-Duct", ASME GT2010-23404.
- [9] Carrotte, J. F., Stevens, S. J. and Wray, A. P., 1990, "The Performance of a Compressor Pre-diffuser Incorporating Compressor Outlet Guide Vanes", AIAA-90-2165.
- [10] "Aggressive Intermediate Duct Aerodynamics for Competitive and Environmentally Friendly Jet Engines (AIDA)", 2004-8, European Union 6th Framework Project, Contract No. AST3-CT-2003502836.
- [11] Ortiz-Duenas, C., Miller, R. J., Hodson, H. P., and Longley, J. P., 2007, "Effect of Length on Compressor Inter-Stage Duct Performance", ASME GT2007-27752.

- [12] Walker, A. D., Barker, A. G., and Carrotte, J. F., 2011, "Integrated OGV Design for an Aggressive S-Shaped Compressor Transition Duct", ASME GT2011-45627.
- [13] Wallin, F., and Eriksson, L., 2006, "Response Surface-Based Transition Duct Shape Optimisation", ASME GT2006-90978.
- [14] Naylor, E. M. J., Ortiz-Duenas, C., Miller, R. J., and Hodson, H. P., 2010, "Optimisation of Non-Axisymmetric Endwalls in S-Shaped Ducts", ASME J. of Turbomachinery, 132(1), pp. 011011-1-10.
- [15] Santer, C., Gottlich, A., Marn, A., Hubinka, J., and Paradiso, B., 2010, "The Application of Low-Profile Vortex Generators in an Intermediate Turbine Diffuser", ASME GT2010-22892.
- [16] Walker, A. D., Denman, P. A. and McGuirk, J. J., 2004, "Experimental and Computational Study of Hybrid Diffusers for Gas Turbine Combustors". ASME J. of Eng. for Gas Turbines and Power, 126(4), pp. 717-725.
- [17] Walker, A. D. and Denman, P. A., 2005, "Hybrid Diffusers For Radially Staged Combustion Systems". AIAA J. of Propulsion and Power, 21 (2), pp. 264-273.
- [18] Camp, T. R. and Shin, H. -W., 1995, "Turbulence Intensity and Length Scale Measurements in Multistage Compressors", ASME Journal of Turbomachinery, Vol. 117(1), pp. 38-46.
- [19] Cumpsty, N. A., 1989, "Compressor Aerodynamics." Longman Scientific and Technical.
- [20] Wray, A. P. and Carrotte, J. F., 1993, "The Development of a Large Annular Facility for Testing Gas Turbine Combustor Diffuser Systems", AIAA-93-2546.
- [21] White, F. M., "Fluid Mechanics", 3rd Ed. 1994. McGraw-Hill, ISBN 0-07-113765-3, pp. 407-410.